Journal of Artificial Intelligence and Data Mining (JAIDM), Vol. 9, No. 1, 2021, 19-29.

Shahrood University of Technology

Journal of Artificial Intelligence and Data Mining (JAIDM)
Journal homepage: http://jad.shahroodut.ac.ir

Research paper

Bio-inspired Computing Paradigm for Periodic Noise Reduction in Digital Images

Najmeh Alibabaie and Ali Mohammad Latif *

Computer Engineering Department, Yazd University, Yazd, Iran.

Article Info

Article History:
Received 03 February 2020
Revised 02 April 2020
Accepted 06 July 2020

DOI:10.22044/jadm.2020.9358.2071

Keywords:
Image Noise Removal, Periodic Noise, Spectrogram, Genetic Algorithm.

**Corresponding author: Alatif@yazd.ac.ir(A. M. Latif).*

Abstract

Periodic noise reduction is a fundamental problem in image processing, which severely affects the visual quality and the subsequent application of the data. Most of the conventional approaches are only dedicated to either the frequency or the spatial domain. In this research work, we propose a dual-domain approach by converting the periodic noise reduction task into an image decomposition problem. We introduce a bio-inspired computational model to separate the original image from the noise pattern without having any a priori knowledge about its structure or statistics. Experiments on both the synthetic and non-synthetic noisy images are carried out in order to validate the effectiveness and efficiency of the proposed algorithm. The obtained results demonstrate the effectiveness of the proposed method both qualitatively and quantitatively.

1. Introduction

A digital image is created in digital image acquisition from a physical scene. In this process, any random variation of the pixel value or color is known as the image noise [1]. Periodic noise is one type of image noise. It is generated by electrical or magnetic interference [2]. This noise can be seen in some visual applications such as medicine [3], traffic control [4], remote sensing [5, 6], television [7], and real-time applications. Due to its frequent occurrence, periodic noise removal is one of the important issues in image processing. In the spatial domain, periodic noise appears as a repetitive pattern on the image and degrades the image quality. Periodic noise not only sharply degrades the image quality in the visual effect but also risks its suitability for the subsequent processing, e.g. image un-mixing and classification. Thus, periodic noise must be removed, and image quality must be improved before the subsequent interpretation.

Periodic noise for an image of size $M \times N$ is spatially modeled through the summation of a total S number of sinusoids with different parameters [8], as follows:

$$n(x,y)=\sum_{i=1}^{S} A_i \sin\begin{pmatrix}\left[2\pi u_{0i}\left(x+B_{xi}\right)/M\right]\\ +\left[2\pi v_{0i}\left(y+B_{yi}\right)/N\right]\end{pmatrix} \tag{1}$$

where A_i denotes the amplitude, u_{0i} and v_{0i} are the i^{th} sinusoidal frequency along the axes x and y, and B_{xi} and B_{yi} are the phase displacements with respect to the origin and $S \in Z^+$.

Periodic noises are often represented by the unintended and the spurious repetitive patterns. These patterns cover the entire image in the spatial domain. Conversely, these are, by nature, well-localized in the corresponding Fourier domain image spectrum.

Remove the periodic noise structures from noisy images efficiently, though the spatial domain filtering techniques confront several troubles (blurred outputs/artifacts, etc.) To the contrary, noisy spectral components can easily be notified by the Fourier domain-based operations. Periodic noises appear as spiky-peaks/star-shaped peak areas in the corresponding image spectrum.

The goal of this research work was to exploit the capability of the spatial and spectral methods to construct a dual-domain method in order to eliminate global periodic noise. Hence, the term dual-domain: spectral decomposition is done in the frequency domain and the results obtained are sent to the next phase for the spatial domain operations.
The structure of this paper is organized as follows. In the next section, a review on some conventional periodic noise reduction algorithms is presented. The proposed method is described in the third section. Comparison results between the proposed algorithm and some conventional methods are given and discussed in the fourth section. The final section presents the conclusion.

2. Literature Review

Periodic noise is divided into the global, local, and stripping categories [9]. In general, the periodic noise reduction methods are divided into two categories: spatial-based approaches and spectral approaches.
Spatial-based approaches can be categorized into several main groups. The first family uses the statistical property of the data. The main idea in these methods is to correct the distribution of the sensors to a reference distribution [10]. As typical examples, moment matching [11] and histogram modification [12] are the relatively early methods in this group. The second family of spatial methods are considered as an ill-posed inverse problem [13]. They are based on constraining image via some regularization terms and estimating it from the noisy image. As examples, maximum a posteriori framework [14], low-rank matrix recovery [15] and unidirectional total variation and sparse representation [16] are the methods in this group.
While the spatial methods have already proved their efficiency for de-striping applications, they have rarely been used for global and local periodic noise reduction. The soft morphological filter is a spatial method introduced for global periodic noise [17].
Despite the dispersion of periodic noise in the spatial domain, it is concentrated in one or more adjoining coefficients in the frequency domain. Thus, spectral methods are usually preferred.
In the frequency domain, noise reduction is performed in two steps. The first step is to find the location of the noisy frequencies. The second step is how to repair the noisy frequencies and to get the restored image. Spectral approaches can be divided into sub-categories according to the function they provide.
The first subcategory consists of the algorithms that try to detect the peaks such as the threshold-based methods [2, 18, 19], histogram analysis-based methods [8], clustering-based methods [20], spectral modeling methods [21, 22], and statistical-based methods [6, 23-27].
The second subcategory consists of the algorithms that try to repair noise frequencies, for example, windowed Gaussian notch filter [19, 24, 27], Gaussian-star filter [28], Sinc-based filter [8, 29, 30] and replacement with zero [20, 23], median [22, 25], minimum [2] value of the neighbors.

3. Proposed Method

The major elements of the proposed method are as follow:

- A 2D spectrogram of image
- A weakened version of the noise-less image
- An intensified version of the periodic noise pattern
- An image decomposer with a Genetic Algorithm (GA) optimizer

The diagram of the proposed method is shown in figure 1, and it is described in the following sub-sections.

3.1. Short-Time Fourier Transform (STFT)

In the literature, STFT has been used to separate audio signals. In these references, the Short-Time Fourier Transform (STFT) is applied to the observed signals for two reasons:

1. The non-stationary property of audio signals
2. To get a sparse representation of the data

However, in our work, the STFT method was taken into account for computational resources (computing time and memory space), which permit reducing the computation complexity and a shorter length for the chromosomes.
Space/frequency representation of a 1-D signal is necessarily a 2-D function of x and frequency u since it must show a 1-D frequency distribution for every point in the signal. Of course, it can represent an image as a vector. However, in this case, it loses information about the pixels neighborhood, and the spectral peaks are not similar, especially at the junction of rows (columns). Furthermore, we have to take into account the peak similarity and the computational complexity considerations simultaneously. Thus, we present a configured spectrogram corresponding to the image signal

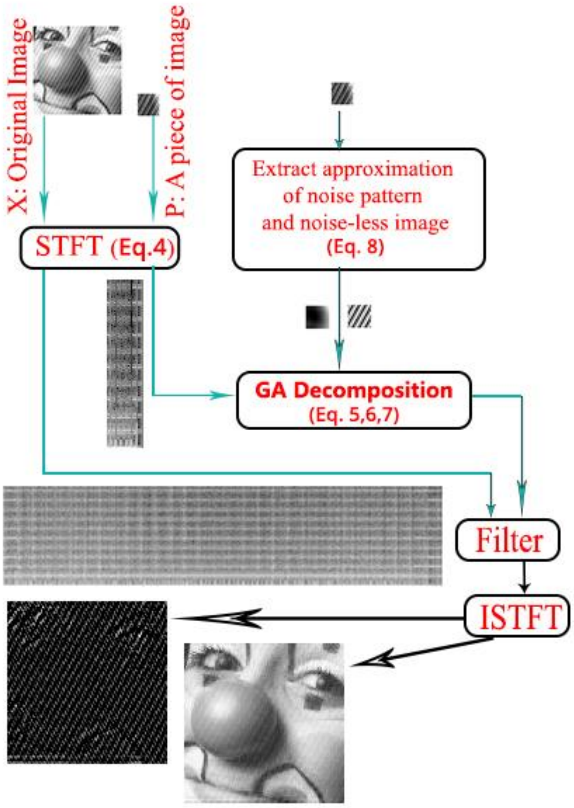

Figure 1. Schematic representation of the proposed method.

3.1.1. Spectrogram of an Image

If the original signal were a 2-D function of x and y (an image), then the space/frequency representation would be a 4-D function of x and y and two frequencies, u and v.

In practice, a set of overlapping patches span the whole image. For each point in the image, a square neighborhood of the surrounding pixels is extracted. Each patch is transformed into the frequency domain using the 2-D Fourier transform. Then each spectrum is converted into a vector representation and form the spectrogram columns.

Then the complex-valued STFT is decomposed into the magnitude and phase components. Due to the symmetry property of the Fourier transform, only half of the Fourier space can be used in the next step.

3.2. Decomposition with a GA optimizer

Genetic algorithm is a meta-heuristic search and optimization technique based on the principles present in natural evolution [31]. It has been successfully used in many optimization problems [32]. In a genetic algorithm, a population of candidate individuals is evolved toward better individuals for an optimization problem

3.2.1. Chromosome Representation

The spectrogram consists of Fourier transforms of image patches with similar noise pattern. Thus, all columns of the spectrogram have similar peaks. The goal is to decompose the spectrogram into the periodic noise and restored image spectrogram.

The number of genes in a chromosome is equal to the number of rows in the spectrogram and the value of each component is a random number in $[0\ \ ]$. Of course, it should be noted that the number of spectrogram rows in the GA block is half of the original spectrogram rows. In fact, the symmetry property of the Fourier transform yields the chromosomes with a shorter length, and therefore, it gives the algorithm memory efficiency

3.2.2. Initialization of Population

An efficient population initialization plays an important role in the process of solving a problem based on GA. Often, the initial population is generated randomly allowing the entire range of possible solutions in the search space. Thus, each component of a chromosome can have an arbitrary value from $[0\ \ ]$.

The proposed method emphasizes a faster convergence speed and reducing the number of generations, so the initial population manner has been carried out to increase the quality of the initial population as follows:

$$S_{abs}(i)=\sum_{j=1}^{Q} V(i,j), i=1,2,\ldots,P \tag{2}$$

$$Peaks = findpeaks(S_{abs})$$

$$Locs=\{Peaks-1, Peaks, Peaks+1\}$$

$$C_k=\begin{bmatrix}1\\1\\\vdots\\1\end{bmatrix}_{P\times 1}$$

$$C_k(locs)=rand()$$

where V is the magnitude spectrogram of size $P\times Q$, and S_{abs} is the row summation of V.

Equation (2) is used to highlight the noisy peak positions. $Peaks$ determines the peak positions in S_{abs}. $Locs$ is the genes that have a non-zero value in the chromosome and consist of peak position and its previous and next position. $C(k)$ is the k^{th} chromosome of the initial population whose values is 1 in all elements except that its $Locs$ positions are replaced by random values.

3.2.3. Decoding Chromosome

In order to decode the chromosomes, the chromosome values is multiplied by the spectrogram columns. The resulting spectrogram is converted to its original size by conjunction operation and then transferred to the spatial domain.

This process should be repeated again with the value of $1-C(k)$ but, in this work, the restored image is obtained from subtracting the noise pattern from the noisy image. This is, of course, to reduce the computational burden. Thus at this stage, an estimation of periodic noise pattern and the restored image is obtained in the spatial domain.

3.2.4. Fitness Evaluation

The solutions will be evaluated in the spatial domain. For this purpose, an approximation of the noise pattern and restored image are used as a base. The fitness for a given chromosome i is:

$$Fit(i)=1/\left[F_1(i)+F_2(i)+F_3(i)\right] \tag{3}$$

$$F_1(i)=1-\frac{\left[\left(\sum_m\sum_n\left(N_{Apr.}(i)_{mn}-\overline{N_{Apr.}}\right)\left(CN(i)_{mn}-\overline{CN(i)}\right)\right)\right]}{\left(\sqrt{\sum_m\sum_n\left(N_{Apr.}(i)_{mn}-\overline{N_{Apr.}}\right)^2\sum_m\sum_n\left(CN(i)_{mn}-\overline{CN(i)}\right)^2}\right)}$$

$$F_2(i)=1-\frac{\left(\sum_m\sum_n\left(R_{Apr.}(i)_{mn}-\overline{R_{Apr.}}\right)\left(CR(i)_{mn}-\overline{CR(i)}\right)\right)}{\left(\sqrt{\sum_m\sum_n\left(R_{Apr.}(i)_{mn}-\overline{R_{Apr.}}\right)^2\sum_m\sum_n\left(CR(i)_{mn}-\overline{CR(i)}\right)^2}\right)}$$

$$F_3(i)=1-\frac{\left(\sum_m\sum_n\left(CN(i)_{mn}-\overline{CN(i)}\right)\left(CR(i)_{mn}-\overline{CR(i)}\right)\right)}{\left(\sqrt{\sum_m\sum_n\left(CN(i)_{mn}-\overline{CN(i)}\right)^2\sum_m\sum_n\left(CR(i)_{mn}-\overline{CR(i)}\right)^2}\right)}$$

where $CN(i)$ is the noise pattern obtained from the i^{th} chromosome, $CR(i)$ is the restored image obtained from the i^{th} chromosome, $N_{Apr.}$ is the approximated noise pattern, $R_{Apr.}$ is the approximated restored image, $F_1(i)$ shows the similarity of $CN(i)$ and $N_{Apr.}$, $F_2(i)$ shows the similarity of $CR(i)$ and $R_{Apr.}$, and $F_3(i)$ shows the similarity of $CR(i)$ and $CN(i)$. The goal is to maximize the fitness function.

The goal is that the periodic noise pattern extracted from the chromosome is similar to the basic (approximated) noise pattern, and the noise-less image extracted from the chromosome is similar to the basic (approximated) noise-less image. On the other hand, the noise pattern should not be seen in the recovered image, so the two images extracted from the chromosome should not be as similar as possible.

3.2.5. Genetic Operators

Selection: selection strategy exploits the fitness information to guide the search into promising search space regions. In this work, the roulette-wheel is used for selection.

Cross-over: cross-over is usually the most important operator to explore the search space. In this work, we employ the affine cross-over operator as follows:

$$\begin{aligned} O_1 &= \lambda_1 P_1+\lambda_2 P_2 \\ O_2 &= \lambda_1 P_2+\lambda_2 P_1 \\ \lambda_1,\lambda_2 &\in \mathrm{R},\ \lambda_1+\lambda_2=1 \end{aligned} \tag{4}$$

where O_1 and O_2 are the parents, and P_1 and P_2 are the offsprings; λ_1,λ_2 are used to compute the weighted average of two vectors.

Mutation: mutation is used to maintain genetic diversity from one generation of a population to the next. In the proposed method, the mutation may be applied to the individuals in two ways: one gene in a chromosome is changed with probability 0.5 and a new chromosome is added to the population with probability 0.5.

3.3. Filtering and Inverse Short Time Fourier Transform (ISTFT)

In this step, the separator is taken from the GA block and used to separate the original noisy image spectrogram. Finally, the algorithm performs inverse short time Fourier transform to reconstruct the restored image.

3.4. Approximation of Periodic Noise Pattern

The approximate noise pattern can be obtained using the following equation:

$$R=\left(Fimage\ \times conj\left(Fimage\right)\right)\ \times sign\left(Fimage\right) \tag{5}$$

where $Fimage$ is the Fourier transform of a corrupted image and $\times$ denotes the element-wise multiplication (also called the Hadamard product). The reason behind using (5) can be explained as follows: a noisy image includes clear peaks in its spectrum. The mentioned relationship increases the magnitude of frequency, and as a result, increases the noise peaks, and consequently, the noise strength. In this way, we can obtain an approximation of the periodic noise pattern in the spatial domain. Figure 2 shows the approximation of a sample noise pattern. In this figure, a sample image is contaminated with periodic noise. $NoiseHat(R)$ is the noise pattern derived from (5).

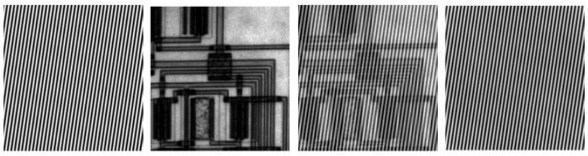

(a) Noise Pattern (b) Original Image (c) Noisy Image (d) Noise Hat

Figure 2. Calculating (5) to create an approximation of the noise pattern.

3.5. Approximation of Restored Image

LFR contains smooth information of the image itself. Equation (5) can also be used to obtain the restored image approximation because LFR in the R spectrum magnitude is also high. On the other hand, Fourier transforms of a noisy image contain the image details and the noise components.

In order to obtain an approximation of the noise-less image, the noisy spectrum is used, and LFR values are gradually increased from the initial values. This increase is achieved using the LFR values of the R spectrum until the noise pattern does not appear on the image.

In fact, if the LFR components of the noisy image spectrum are replaced by the LFR components of R, gradually a very smooth version of the restored image will be formed, and after a while, the noise pattern will emerge.

4. Implementation and Experimental Results

The proposed method was implemented in the MATLAB environment. All simulations were run on a PC computer with Intel Dual Core 2.50 GHz processor and 4GB RAM. The performance of this method was objectively and subjectively assessed with other state-of-the-art algorithms in term of the Mean Absolute Error (MAE) [33], Peak Signal-to-Noise Ratio ($PSNR$) [22], mean Structural Similarity Index Measure ($SSIM$) [34], and Edge Accuracy ($EAcc$) and precision ($EPrec$).

4.1. Accuracy and Precision of Edge Pixels

One of the obvious effects of the periodic noise is seen on the edge pixels, i.e. periodic noise may introduce some extra edges or destroy some of the edges. A good restoration algorithm must be able to remove the undesired edges and to reconstruct the decayed ones. In this case, the restored edge-map approaches closer to the original edge-map. Hence, the performance of the restoration algorithms can also be evaluated in terms of the edge accuracy ($EAcc$) and edge precision ($EPrec$) [29]. For calculating those parameters, we need the information about the true edge points and false edge points. Here, the Canny method is employed for edge detection. If f and $\hat{f}$ are the noise-less image and the restored image of size $M \times N$, respectively, these objective performance metrics are defined by:

$$EAcc = \frac{\sum_{x=1}^{M}\sum_{y=1}^{N}\left[T_{\varepsilon}+T_{n\varepsilon}\right]}{M \times N} \tag{6}$$

$$EPrec = \left(\frac{\sum_{x=1}^{M}\sum_{y=1}^{N}\left[T_{\varepsilon}\right]}{\sum_{x=1}^{M}\sum_{y=1}^{N}\left[T_{\varepsilon}+F_{\varepsilon}\right]}\right)$$

$$T_{\varepsilon} = \begin{cases} 1 & if\ O\left(f,\hat{f}\right)=1\ and\ R\left(f,\hat{f}\right)=1 \\ 0 & otherwise \end{cases}$$

$$T_{n\varepsilon} = \begin{cases} 1 & if\ O\left(f,\hat{f}\right)=0\ and\ R\left(f,\hat{f}\right)=0 \\ 0 & otherwise \end{cases}$$

$$T_{F} = \begin{cases} 1 & if\ O\left(f,\hat{f}\right)=0\ and\ R\left(f,\hat{f}\right)=1 \\ 0 & otherwise \end{cases}$$

where O and R are the edge images of the original image (f) and the restored image, ($\hat{f}$) respectively. An efficient algorithm in noise reduction would have a high value of $SSIM$, $PSNR$, $EAcc$, and $EPrec$ and a low value of MAE.

The performance of the proposed method is compared with Windowed Adaptive Switching Minimum Filter (WASMF) [21], Adaptive Threshold Based Frequency domain filter (ATBF) [2], Laplacian-based Frequency Domain Filter (LFDF) [22], Median filter in spectral domain (Median) [25], Mean filter in spectral domain (Mean) [23], Windowed Gaussian Notch Filter (WGNF) [24], Adaptive Gaussian Notch Filter (AGNF) [19], Adaptive Optimum Notch Filter (AONF) [18], A-Contrario Automated Removal of quasi-Periodic noise using frequency domain statistics (ACARP) [7], Automated Removal of quasi-Periodic noise using frequency domain statistics (ARP) [27], soft morphological filter (SMF) [17], Adaptive Sinc Restoration Filter (ASRF) [29]. Table 1 shows the parameters of the compared methods.

5. Results and Discussion

The proposed method was tested in several steps, as follow:

- Synthetic periodic noise
  - Low-frequency periodic noise
  - High-frequency periodic noise
  - Multi-frequency periodic noise
- Non-synthetic periodic noise

Afterward, the computational complexity analysis of the proposed method is discussed. The synthetic corrupted images are created by adding artificially the generated sinusoidal noise patterns to the uncorrupted reference images. The performance of spectral domain techniques is strongly dependent on the test image and the noise parameters; therefore, the results were averaged over the 20 repetitions under the test conditions. In all tests, the test images were 256×256 pixels.

In the experiments, to implement STFT in spectrogram generation, the window is of the rectangular type and its length has been set to 21×21 and overlapping size of 10 for both dimensions.

In all tables, the "noisy image" column was added to evaluate the quality of the degraded noisy image. For that, the performance values are averaged for each set of noisy images.

Table 1. Parameters of the compared methods.

Method	Parameter	Value
Mean	Window size	11×11
	threshold	7
	Normalizing Divider	50
Median	Window size	11×11
	Threshold	7
WGNF	Window size	11×11
	Threshold	7
	A	0.1
	B	1.0
ARP	Patch size	128
ACARP	Patch size	128
	logNFAthresh	0
WASMF	C_1	0.4
	C_2	1.1
ATBF	alpha	1.8
LFDF	C_1	0.4
	C_2	1.1
	γ	0.9
AGNF	w	3
	A	1.0
	B	0.01
AONF	w	3
SMF	Structure element size	5
ASRF	C_1	10
	C_2	2.5
	Structure element size	5
	Smallest filtering window(P)	2
Proposed Method	Number of Iteration	100
	Pop. size	60
	Crossover rate	0.8
	Mutation rate	0.2

5.1. Synthetic Periodic Noise

5.1.1. Low-frequency Periodic Noise

In this step, the low-frequency periodic noise structures are considered as a noise source. In this case, the simulations are carried out on the images with noise pattern of (1) with $u_0, v_0 \subseteq [2,14]$. The simulation results are shown in table 2.

At this step, a number of spatial methods, spectral methods, and spectral-spatial methods were considered. Most of the spectral methods exclude a specific region from detection by selecting the LFR radius. This radius may not be optimum. It decreases their performance in face of low-frequency periodic noise. The methods like SMF perform only spatial operations. They are associated with a small improved outcome but they have no viewpoint about the noise pattern and the original image.

5.1.2. High-frequency Periodic Noise

In this step, high-frequency periodic noise structures are considered as a noise source. In this case, the simulations are carried out on the images with noise pattern of (1) with $u_0, v_0 > 20$. The simulation results are shown in table 3. It is clearly evident from tables 2 and 3 that the restoration algorithms have a better performance in high-frequency periodic noise fading.

In table 3, the proposed method is also compared with the spectral, spatial, and spectral-spatial methods. Increasing noise power tends to decrease the performance of the spatial-domain methods regardless of frequency bands.

The concentration of periodic noise in one or more adjacent coefficients in the frequency domain causes the spectral approaches to be simpler than the spatial method. These methods face other challenges yet. A noisy image at best is pure periodic noise that affects only a frequency component. Reconstructing the noisy image is done by reinstating this component. In a more complex case, periodic noise will be quasi-periodic noise. In other words, when the bandwidth of the periodic noise increases, several rows or columns of the spectrum may be involved. In this case, detecting the fundamental frequency and its harmonics of the periodic noise is also a challenging task.

Table 3 shows that the proposed algorithm outperforms the most recent state-of-the-art algorithms.

5.1.3. Multi-frequency Periodic Noise

Generally, the restoration algorithms work well for a single frequency periodic noise but multi-frequency periodic noise fading is a challenging problem. Most of the non-synthetic images are also corrupted by the multi-frequency periodic noise.

Table 2. Comparison amongst different restoration algorithms for restoring sample images corrupted by low-frequency periodic noise in terms of performance metrics.

Type	Image	Amplitude	Performance metric	Noisy Image	WASMF	LFDF	AONF	ACARP	ARP	SMF	ASRF	GA
Low frequency Periodic Noise	Lena	0.9	**PSNR**	13.85	13.84	14.63	12.42	16.10	15.95	14.20	15.83	16.26
			SSIM	0.374	0.370	0.434	0.302	0.570	0.567	0.239	0.563	0.531
			MAE	17.01	17.00	15.24	20.96	12.20	12.60	16.34	12.96	11.81
			EAcc.	0.261	0.246	0.284	0.225	0.443	0.405	0.093	0.318	0.449
			EPrec.	0.824	0.820	0.842	0.818	0.881	0.883	0.785	0.889	0.893
	Lake	0.6	**PSNR**	15.56	15.69	15.87	14.37	17.53	17.59	15.20	16.11	17.77
			SSIM	0.509	0.507	0.524	0.424	0.641	0.623	0.281	0.569	0.705
			MAE	17.61	17.60	16.97	19.91	14.33	14.67	17.96	16.70	13.80
			EAcc.	0.330	0.323	0.335	0.268	0.352	0.370	0.098	0.395	0.403
			EPrec.	0.831	0.829	0.837	0.813	0.854	0.846	0.776	0.838	0.854

Table 3. Comparison amongst different restoration algorithms for restoring sample images corrupted by high-frequency periodic noise in terms of performance metrics.

Type	Image	Amplitude	Performance metric	Noisy Image	ATBF	LFDF	AONF	Mean	WGNF	SMF	AGNF	GA
High frequency Periodic Noise	Barbara	0.3	**PSNR**	20.32	25.45	24.22	19.84	25.39	24.35	22.09	28.21	28.54
			SSIM	0.419	0.731	0.666	0.408	0.727	0.861	0.637	0.875	0.916
			MAE	10.91	5.72	6.98	11.15	5.82	6.41	7.93	3.98	3.91
			EAcc.	0.649	0.777	0.607	0.580	0.785	0.820	0.337	0.837	0.882
			EPrec.	0.894	0.947	0.908	0.880	0.952	0.958	0.855	0.966	0.975
	Lena	0.9	**PSNR**	13.90	17.85	15.33	13.80	17.50	17.75	16.67	17.90	18.16
			SSIM	0.157	0.545	0.292	0.154	0.469	0.560	0.571	0.518	0.574
			MAE	17.39	8.60	14.27	17.60	9.79	9.12	9.25	9.01	8.40
			EAcc.	0.824	0.816	0.606	0.611	0.825	0.771	0.419	0.832	0.866
			EPrec.	0.941	0.971	0.899	0.899	0.971	0.960	0.883	0.967	0.980

Table 4. Comparison amongst different restoration algorithms for restoring sample images corrupted by multi-frequency periodic noise in terms of performance metrics.

Type	Image	Performance metric	Noisy Image	ATBF	LFDF	AONF	Mean	WGNF	SMF	AGNF	ASRF	GA
Multi frequency Periodic Noise	Boat	**PSNR**	19.39	23.29	20.98	17.95	23.34	22.76	20.20	23.47	23.60	23.80
		SSIM	0.374	0.668	0.512	0.331	0.654	0.702	0.499	0.676	0.712	0.738
		MAE	9.45	5.02	7.42	17.07	5.14	4.95	7.80	4.95	4.65	4.46
		EAcc.	0.644	0.795	0.614	0.526	0.778	0.709	0.271	0.741	0.813	0.831
		EPrec.	0.905	0.949	0.907	0.876	0.923	0.894	0.825	0.933	0.945	0.979
	Lena	**PSNR**	17.80	19.70	18.39	17.90	19.84	18.53	18.25	19.93	20.14	20.34
		SSIM	0.355	0.547	0.424	0.362	0.546	0.583	0.533	0.568	0.639	0.643
		MAE	8.66	5.83	7.81	19.88	5.84	7.39	7.67	5.64	5.30	5.12
		EAcc.	0.624	0.623	0.594	0.567	0.604	0.590	0.298	0.625	0.658	0.687
		EPrec.	0.923	0.923	0.916	0.910	0.934	0.928	0.857	0.923	0.946	0.961

In this simulation, the reference images are added with multi-frequency periodic noise. In this case, the simulations are carried out on the images with noise pattern of (1) with $S \subseteq \{1,2,3,4,5\}$. The simulation results are shown in table 4.

5.2. Non-Synthetic Periodic Noise

The performance of the proposed method is evaluated in a real situation. In this case, the images from various fields, contaminated with different types of non-synthetic periodic noise structures are tested as a benchmark.

As the distortion-free reference image is not within reach, the performance evaluation metrics cannot be computed. Hence, the performance is compared visually only. Figure 3 shows the restored outputs of the proposed algorithm, while restoring a few non-synthetically corrupted images.

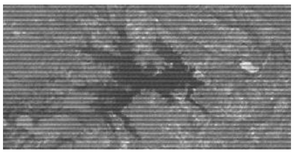

a. Stripping image

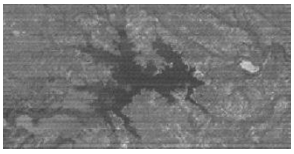

b. Restored Stripping image

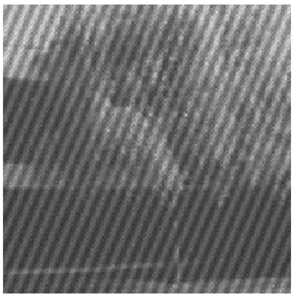

c. Noisy Tree

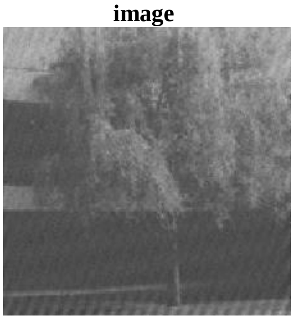

d. Restored Tree

e. Noisy woman

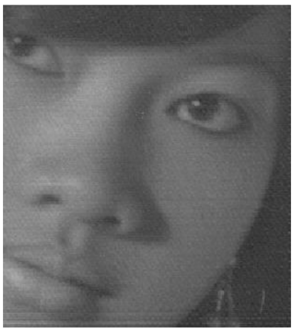

f. Restored woman

Figure 3. Real images corrupted by different non-synthetic periodic noise structures, and restored images using the proposed method.

5.3. Periodic Noise Removal in RGB Images

The proposed method can easily generalize from grayscale images to RGB images. For this purpose, image planes are separated from each other.

Then the periodic noise reduction method is applied to each separated plane. The final RGB image is obtained from a combination of these results. Figure 4 shows the restored outputs of the proposed algorithm while restoring the corrupted color image.

6. Computational Resource Analysis

In the proposed method, some considerations have to be taken into account for computational resources (computing time and memory space), as follows.

6.1. Memory Space Analysis

Memory consumption analysis can be used to identify the memory resources that are allocated and released over time. Let decomposition of a noisy image of size $M \times N$ be considered. If the number of populations in GA is Pop and the cross-over rate is cr and the mutation rate is mr, then a generation requires $Memory = M \times N \times (Pop \times (cr + mr + \ ))$. In the proposed method, STFT is used in order to improve the memory consumption. In this case, the overlapping patches and their spectrum are considered of size $p \times q$. Due to the symmetry property of Fourier transform, a chromosome will have $CM = (p \times q)$ genes. Thus for the mentioned example, a generation requires $Memory = M \times N \times (Pop \times (cr + mr + \ ))$.

6.2. Computing Time Analysis

If fast Fourier transform is used, the complexity would be $O(\ p \times q \times log\ p \times q)$ [35] for a patch of size $p \times q$. Each spectrogram column is obtained from the 2-D Fourier transform of a patch. Periodic noise appears on all spectrogram columns as similar peaks. The whole spectrogram is decomposed in fitness evaluation, while in the implementation, the emphasis is on computational efficiency. Computational efficiency is achieved through the selection of a Part Of the Image (POI) in fitness evaluation. Since periodic noise is scattered throughout the whole image, the selecting of a part of the whole taken as representative of the whole image. POI like the original image has similar peaks on its spectrogram but the number of their columns is different. Therefore, if a separator chromosome can decompose the POI spectrogram correctly, it will also be able to decompose the original spectrogram along with improving the computational efficiency and saving the computational time.

If the POI spectrogram of size $M_1 \times N_1, M_1 < M, N_1 < N$ is used in the GA block and the hop size is $a \times b$, the complexity of the ISTFT would be equal to $O(M/a \times N\ b \times p \times q \times log(pq))$. The running time for a generation with the number of population Pop and the crossover rate cr and the mutation rate mr and number of iteration Itr is as follows:

$$\theta(T2)=\left(Pop+Pop\left(cr+mr\right)\right)\times Itr\times\left(M_1/a\right)\times\left(N_1/b\right)\times p\times q\times\log\left(pq\right)$$

7. Conclusion

In this work, blind periodic noise decomposition from digital images was proposed using a genetic algorithm (GA). In the proposed method, the frequency and spatial domain image information can be considered and optimized in GA simultaneously. On the other, GA in the problem of periodic noise reduction faces challenges in terms of computational resources. However, the use of image characteristics and optimization in the area can also be useful for solving periodic noise reduction. Both of the advantages and disadvantages of GA are formulated in the proposed method in such a way that its disadvantages are minimized and its advantages are used. Nonetheless, a fully automatic method for periodic noise reduction is preferred, which will be considered in the future research work.

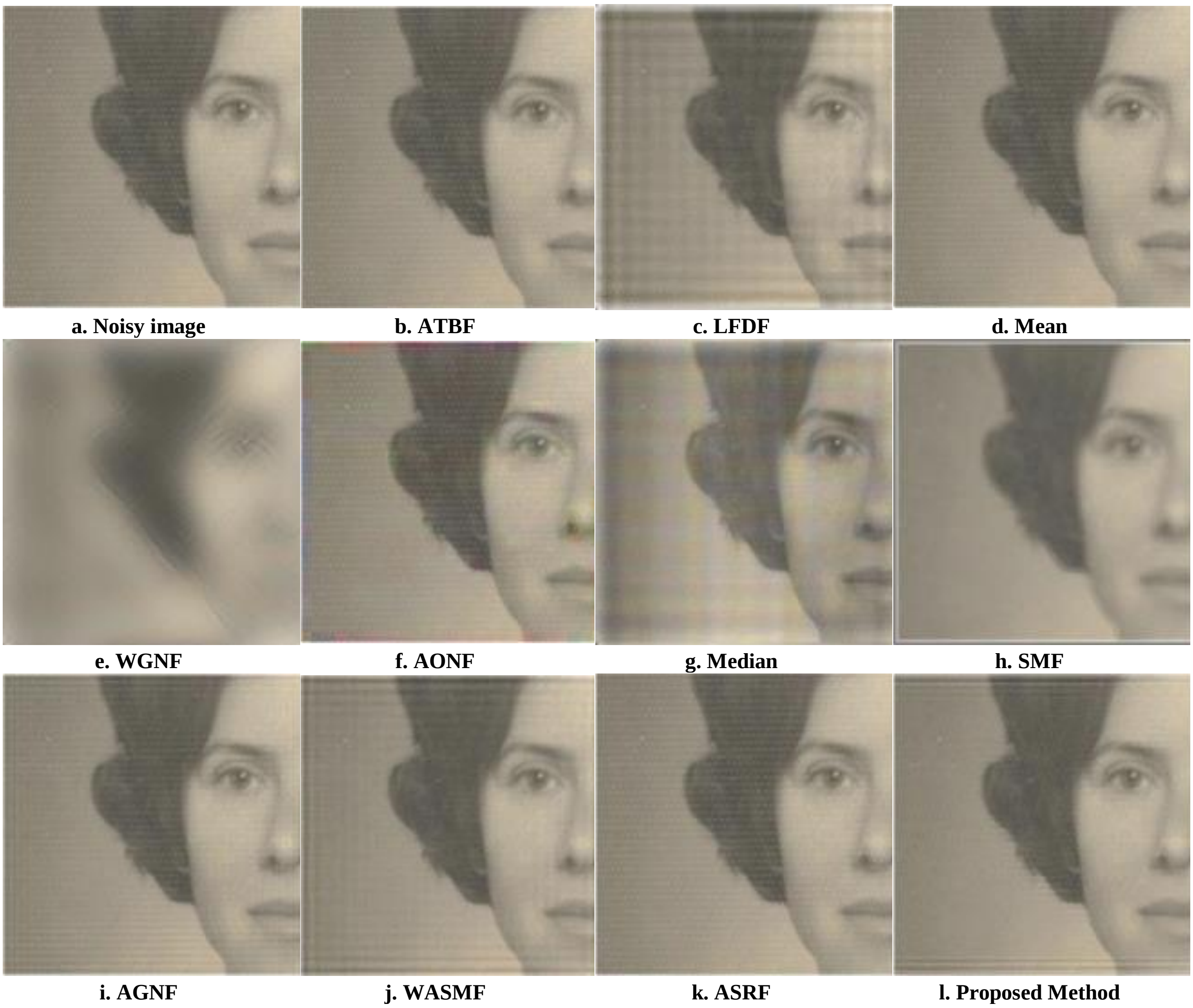

Figure 4. Visual comparisons for different de-noising algorithms for a non-synthetically corrupted image Oldprintwoman.

References

[1] R. C. Gonzalez, R. Woods, *Digital image processing*, 3rd Edition ed., Prentice Hall, 2007.

[2] J. Varghese, "Adaptive threshold based frequency domain filter for periodic noise reduction". *AEU - international journal of electronics and communications*, vol. 70(12), pp. 1692-1701, 2016.

[3] A. Carvalho, T. Esteves, P. Quelhas, F. J. Monteiro, "Mobilityanalyser: A novel approach for automatic quantification of cell mobility on periodic patterned substrates using brightfield microscopy images", *Computer methods and programs in biomedicine*, vol. 162(1), pp. 61-67, 2018.

[4] M. M. Ata, M. El-Darieby, M. Abdelnabi, S Napoleon. "Proposed enhancement for vehicle tracking

in traffic videos based computer vision techniques", *International journal of advanced intelligence paradigms*, vol. 2019, 2018.

[5] Y. Chen, T. Z. Huang, X. L. Zhao, L. J. Deng, J. Huang, "Stripe noise removal of remote sensing images by total variation regularization and group sparsity constraint", *Remote sensing*, vol. 9(6), pp. 559. 2017.

[6] F. Sur, An a-contrario approach to quasi-periodic noise removal. *International conference on IEEE image processing, Quebec City*, Canada, 2015, pp. 3841-3845.

[7] R. D. Smith, *Digital transmission systems* (3rd Edition). Heidelberg Springer science and business media, 2012.

[8] D. Chakraborty, M. K. Tarafder, A. Chakraborty, A. Banerjee, "A proficient method for periodic and quasi-periodic noise fading using spectral histogram thresholding with Sinc restoration filter", *AEU - international journal of electronics and communications*, vol. 70(12), pp. 1580-1592, 2016.

[9] R. Schowengerdt, *Remote sensing: models and methods for image processing* (3rd Edition), Academic Press, Waltham, 2007.

[10] P. Rakwatin, W. Takeuchi, Y. Yasuoka, Restoration of Aqua MODIS band 6 using histogram matching and local least squares fitting. *IEEE transactions Geoscience and remote sensing*, vol. 47(2), pp. 613-627, 2009.

[11] F. L. Gadallah, G. Csillag, E. J. M. Smith, Destriping multisensory imagery with moment matching. *Remote Sensing*, vol. 21(12), pp. 2505–2511, 2000.

[12] M. Wegener, "Destriping multiple sensor imagery by improved histogram matching". *Remote Sensing*, vol. 11(5), pp. 859—875, 1990.

[13] W. He, H. Zhang, L. Zhang, H. Shen, "Total-variation regularized low-rank matrix factorization for hyper-spectral image restoration", *IEEE transactions Geoscience and remote sensing*, vol. 54(1), pp. 178-188, 2016.

[14] H. Shen, L. Zhang, A map-based algorithm for de-striping and inpainting of remotely sensed images, *IEEE transactions Geoscience and remote sensing*, vol. 47(5), pp. 1492-1502, 2009.

[15] Y. Chang, L. Yan, T. Wu, S. Zhong, "Remote sensing image stripe noise removal: from image decomposition perspective", *IEEE transactions on Geoscience and remote sensing*, vol. 54(12), pp. 7018-7031, 2016.

[16] Y. Chang, L. Yan, H. Fang, H. Liu, "Simultaneous de-striping and de-noising for remote sensing images with unidirectional total variation and sparse representation", *IEEE Geoscience and remote sensing letters*, vol. 11(6), pp. 1051-1055, 2014.

[17] Z. Ji, H. Liao, X. Zhang, Q. Wu, 2006. "Simple and efficient soft morphological filter in periodic noise reduction. In IEEE region 10 conference TENCON, pp. 1–4.

[18] P. Moallem, M. Behnampour, "Adaptive optimum notch filter for periodic noise reduction in digital images", *Amirkabir international journal of electrical and electronics engineering*, vol. 42(1), pp. 1-7, 2010.

[19] P. Moallem, M. Masoumzadeh, M. Habibi, "A novel adaptive Gaussian restoration filter for reducing periodic noises in digital image", *Signal, image and video processing*, vol. 9(5), pp. 1179-1191, 2013.

[20] S. Dutta, A. Mallick, S. Roy, U. Kumar, "Periodic noise recognition and elimination using RFPCM clustering", *International conference on electronics and communication systems, Coimbatore*, 2014, pp. 1-5.

[21] J. Varghese, S. Subash, N. Tairan, Fourier transform based windowed adaptive switching minimum filter for reducing periodic noise from digital images. *IET image processing*, 10(9), 646- 656. 2016.

[22] J. Varghese, S. Subash, N. Tairan, B. Babu, "Laplacian based frequency domain filter for the restoration of digital images corrupted by periodic noise", *Canadian journal of electrical and computer engineering*, vol. 39(2), pp. 82-91, 2016.

[23] I. Aizenberg, C. Butakoff, "Frequency domain median like filter for periodic and quasi-periodic noise removal", *SPIE proceeding, San Jose*, California, United States, 2002, pp. 181-191.

[24] I. Aizenberg, C. Butakoff, "A windowed gaussian notch filter for quasi-periodic noise removal", *Image and vision computing*, vol. 26(10), pp. 1347-1353. 2008.

[25] I. Aizenberg, C. Butakoff, J. Astola, K. Egiazarian, "Nonlinear frequency domain filter for quasi periodic noise removal". *International TICSP workshop on spectral methods and multi-rate signal processing, Toulouse*, France, 2002, pp. 147-153.

[26] F. Sur, "A non-local dual-domain approach to cartoon and texture decomposition", *IEEE transactions on image processing*, vol. 28(4), pp. 1882–1894, 2019.

[27] F. Sur, M. Grédiac, "Automated removal of quasi-periodic noise using frequency domain statistics", *Journal of electronic imaging*, vol. 24(1), pp. 1-19, 2015.

[28] S. Ketenci, A. Gangal, Design of Gaussian star filter for reduction of periodic noise and quasi-periodic noise in gray level images. *International symposium on innovations in intelligent systems and applications, Trabzon*, 2012, pp. 1-5.

[29] D. Chakraborty, A. Chakraborty, A. Banerjee, S. R. B. Chaudhuri, "Automated spectral domain approach of quasiperiodic denoising in natural images using notch filtration with exact noise profile", *IET image processing*, vol. 12(7), pp. 1150–1163, 2018.

[30] D. Chakraborty, M. K. Tarafder, A. Banerjee, S. R. B. Chaudhuri, “Gabor-based spectral domain automated notchreject filter for quasi-periodic noise reduction from digital images”, *Multimedia tools and applications,* vol. 78(2), pp. 1757—1783, 2019.

[31] N. Alibabaie, M. Ghasemzadeh, C. Meinel, A variant of genetic algorithm for non-homogeneous population, *ITM web of conferences, Rome*, Italy, 2017, pp. 1—8.

[32] M. Simeunovic, I. Djurovic, A. Pelinkovic, “Parametric estimation of 2-D cubic phase signals using high-order Wigner distribution with genetic algorithm”, *Multidimensional systems and signal processing*, vol. 30(1), pp. 451–464, 2019.

[33] C. J. Willmott, K. Matsuura, “Advantages of the mean absolute error (MAE) over the root mean square error (RMSE) in assessing average model performance”, *Climate Research*, vol. 30, pp. 79—82, (2005).

[34] Z. Wang, A. Bovik, H. Sheikh, E. Simoncelli, “Image quality assessment: from error visibility to structural similarity”, *IEEE transactions on image processing*, 13(4), 600—612, 2004.

[35] J. Cooley, P. Lewis, P. Welch, “Historical notes on the fast Fourier transform”. *IEEE transactions on audio and electroacoustics*, vol. 15(2), pp. 76–79. 1967.

حذف نویز متناوب از تصاویر دیجیتال با استفاده از یک رویکرد محاسباتی زیست الهام دوگانه

نجمه علی بابایی و علی محمد لطیف*

دانشکده مهندسی کامپیوتر، دانشگاه یزد، یزد، ایران.

ارسال ۲۰۲۰/۰۲/۰۳؛ بازنگری ۲۰۲۰/۰۴/۰۲؛ پذیرش ۲۰۲۰/۰۷/۰۶

چکیده:

نویز متناوب با افزودن الگوهای مشابه بر روی تصویر باعث تخریب کیفیت آن می‌شود. این نویز به صورت پیک‌هایی در طیف فرکانسی تصویر ظاهر می‌شود. جداسازی کور تصاویر ترکیب شده یا همپوشان یکی از مسائل رایج در پردازش تصویر است. این پژوهش بر جداسازی کور نویز متناوب از تصاویر دیجیتال متمرکز است. برای این منظور اطلاعات تصویر در حوزه مکان و فرکانس به طور همزمان مورد توجه قرار می‌گیرد. روال جداسازی کور در الگوریتم ژنتیک انجام می‌شود و در آن عملیات تفکیک در حوزه فرکانس و بهینه سازی تابع معیار در حوزه مکان انجام می‌گردد. در انتها جداساز ارائه شده در حوزه فرکانس بر روی تصویر نویزی اعمال شده و تصویر بازسازی شده به دست می‌آید. ملاحظاتی در زمینه حافظه و زمان انجام شده است که به واسطه آن اندازه جداساز ارائه شده در الگوریتم ژنتیک به اندازه تصویر وابسته نباشد و از طرف دیگر محاسبات موجود در الگوریتم ژنتیک مستقل از اندازه تصویر انجام پذیرد. عملکرد روش پیشنهادی روی تعدادی تصویر محک آغشته به نویز مصنوعی و غیرمصنوعی بررسی گردید. نتایج شبیه‌سازی با استفاده از معیارهای کیفی و کمی حاکی از عملکرد قابل‌قبول آن است.

کلمات کلیدی: حذف نویز تصویر، نویز متناوب، طیف نگاره، الگوریتم ژنتیک.